the plant journal

Involvement of SlSTOP1 regulated *SlFDH* expression in aluminum tolerance by reducing NAD$^+$ to NADH in the tomato root apex

Qiyu He[1,†] , Jianfeng Jin[2,†] , Pengfei Li[1] , Huihui Zhu[1] , Zhanqi Wang[3] , Wei Fan[4,*] and Jian Li Yang[1,*]

[1]*State Key Laboratory of Plant Physiology and Biochemistry, College of Life Sciences, Zhejiang University, Hangzhou 310058, China,*
[2]*Department of Horticulture, Zhejiang University, Zijingang Campus, 866 Yuhangtang Road, Hangzhou 310058, China,*
[3]*Key Laboratory of Vector Biology and Pathogen Control of Zhejiang Province, College of Life Sciences, Huzhou University, Huzhou 313000, China, and*
[4]*College of Horticulture and Landscape, Yunnan Agricultural University, Kunming, China*

SUMMARY

Formate dehydrogenase (FDH; EC 1.2.1.2.) has been implicated in plant responses to a variety of stresses, including aluminum (Al) stress in acidic soils. However, the role of this enzyme in Al tolerance is not yet fully understood, and how *FDH* gene expression is regulated is unknown. Here, we report the identification and functional characterization of the tomato (*Solanum lycopersicum*) *SlFDH* gene. *SlFDH* encodes a mitochondria-localized FDH with K_m values of 2.087 mM formate and 29.1 μM NAD$^+$. Al induced the expression of *SlFDH* in tomato root tips, but other metals did not, as determined by quantitative reverse transcriptase-polymerase chain reaction. CRISPR/Cas9-generated *SlFDH* knockout lines were more sensitive to Al stress and formate than wild-type plants. Formate failed to induce *SlFDH* expression in the tomato root apex, but NAD$^+$ accumulated in response to Al stress. Co-expression network analysis and interaction analysis between genomic DNA and transcription factors (TFs) using PlantRegMap identified seven TFs that might regulate *SlFDH* expression. One of these TFs, SlSTOP1, positively regulated *SlFDH* expression by directly binding to its promoter, as demonstrated by a dual-luciferase reporter assay and electrophoretic mobility shift assay. The Al-induced expression of *SlFDH* was completely abolished in *Slstop1* mutants, indicating that SlSTOP1 is a core regulator of *SlFDH* expression under Al stress. Taken together, our findings demonstrate that SlFDH plays a role in Al tolerance and reveal the transcriptional regulatory mechanism of *SlFDH* expression in response to Al stress in tomato.

Keywords: aluminum toxicity, formate, formate dehydrogenase, NAD$^+$, NADH, transcriptional regulation.

INTRODUCTION

Formate dehydrogenase (FDH; EC 1.2.1.2), a member of the superfamily of D-specific 2-hydroxy acids dehydrogenase (Vinals et al., 1993), catalyzes the oxidation of formate to carbon dioxide (CO_2) coupled with the reduction of NAD$^+$ to NADH. FDHs are classified into two groups based on their structure. Members of the first group, which possess molybdenum or tungsten cofactors and [Fe–S] centers, are heteromeric and have been isolated from anaerobic bacteria and archaea (Ferry, 1990). Members of the second group, which lack cofactors and metals, are homodimeric, and are found in plants, methylotrophic bacteria and yeast (*Saccharomyces cerevisiae*; Labrou &

Rigden, 2001). Due to the practical applications of FDH-catalyzed NADH production and the significance in understanding the dehydrogenase catalytic mechanism, studies on FDH are of great importance (Boyington et al., 1997).

Formate dehydrogenase from plants was first described in pea (*Pisum sativum*) seeds (Davison, 1951; Mathews & Vennesland, 1950). *FDH* in potato (*Solanum tuberosum*) leaves is induced by various stresses, such as hypoxia, chilling, drought and wounding (Hourton-Cabassa et al., 1998). In barley (*Hordeum vulgare*) roots, *FDH* expression is induced by iron deficiency, possibly because oxygen deficiency can result from iron deficiency (Suzuki et al., 1998). The expression of *FDH* is also induced

by the exogenous application of metabolites such as abscisic acid, glycolytic products and formate (Hourton-Cabassa et al., 1998). In addition to the transcriptional regulation of *FDH* genes, translational regulation and posttranslational modifications of FDH proteins have also been described in plants under stress. For example, FDH protein accumulation was induced by copper stress in *Cannabis sativa* roots (Elisa et al., 2007), and by cadmium (Cd) stress in flax (*Linum usitatissimum*) cell cultures (Hradilová et al., 2010). When soybean (*Glycine max*) roots were exposed to various biotic and abiotic stress treatments, FDH accumulated in leaves (Zhao et al., 2013). FDH is the substrate for the RING-type ubiquitin ligase KEEP ON GOING (KEG), which mediates the proteasome-dependent degradation of FDH. Overexpressing *KEG* increased formate sensitivity in Arabidopsis (*Arabidopsis thaliana*), as formate inhibited root elongation more strongly in these plants compared with wild-type (WT; McNeilly et al., 2018). Using a combination of matrix-assisted laser desorption/ionization mass spectrometry and electrospray ionization tandem mass spectrometry, FDH was found to be phosphorylated at residues Thr-76 and Thr-333 (Bykova et al., 2003). However, both the transcriptional and post-transcriptional regulatory mechanisms of *FDH* genes remain largely unknown.

Aluminum (Al) toxicity is a major factor limiting plant growth in acidic soils, which represent approximately 50% of potentially arable lands worldwide (Chen et al., 2022; Kochian et al., 2015). Plants employ different strategies to cope with this toxic metal, depending on its concentration and the exposure time (Barceló & Poschenrieder, 2002). The most well-documented strategies rely on either external exclusion mechanisms or internal tolerance mechanisms (Yang et al., 2019). The former prevent Al from entering root cells, and the latter involve the chelation and compartmentalization of Al once it has entered the cells. Emerging evidence has revealed the importance of the metabolic adaptation of plants in response to Al stress. For instance, in rice bean (*Vigna umbellata*), both oxalate and formate accumulate in response to Al stress, which likely contributes to Al toxicity (Lou, Fan, et al., 2016; Lou, Gong, et al., 2016). Similarly, oxalate accumulated in wild soybean (*Glycine soja*) in response to Al and Cd (Xian et al., 2020). Overexpressing *VuFDH* from rice bean increased the tolerance of transgenic tobacco (*Nicotiana tabacum*) plants to Al toxicity and repressed Al-induced formate accumulation, suggesting that VuFDH confers Al tolerance by degrading formate (Lou, Gong, et al., 2016). Notably, the expression of *VuFDH* was induced by Al stress, as has been also reported for *FDH* in tomato (*Solanum lycopersicum*; Jin et al., 2022) and buckwheat (*Fagopyrum esculentum*; Xu et al., 2017). Therefore, Al stress signaling triggers the expression of *FDH* genes in some plants, paving the way for further revealing the regulatory mechanism of *FDH* expression in plants under stress.

In this present study, we performed bioinformatic and enzymatic characterization of SlFDH from tomato. Furthermore, by generating and analyzing *SlFDH* loss-of-function mutants via clustered regularly interspaced short palindromic repeat (CRISPR)/CRISPR-associated nuclease 9 (Cas9)-mediated genome editing, we demonstrated that SlFDH is involved in Al tolerance in tomato. Additionally, by constructing gene regulatory networks and performing hierarchical clustering analysis via PlantRegMap, we identified SlSTOP1 as a master regulator of *SlFDH* expression. The induction of *SlFDH* expression was completely abolished in *Slstop1* mutants, confirming the role of this transcription factor (TF) in Al tolerance.

RESULTS

Sequence analysis of tomato *SlFDH*

SlFDH (Solyc02g086880) has a coding sequence of 1146 base pairs (bp), which encodes a protein of 381 amino acids. The deduced SlFDH protein has a cleavable and conserved signal peptide in its N terminus, allowing it to enter the mitochondria (Ambard-Bretteville et al., 2003a). AtFDH proteins from Arabidopsis have been detected in both the mitochondria and chloroplasts of leaf cells (Herman et al., 2002). Multiple amino acid sequence alignment of SlFDH with FDH proteins from potato, eggplant (*Solanum melongena*), pepper (*Capsicum annuum*), Arabidopsis and rice bean showed that the signal peptides are the most variable region, but the first three amino acids in the signal peptide are highly conserved (Figure S1). This result is consistent with the finding that removing only the first two amino acids or replacing the second and (especially) third amino acids in this sequence abolished the translocation of FDH into mitochondria (Ambard-Bretteville et al., 2003a).

Phylogenetic analysis indicated that FDH proteins are highly conserved in solanaceous plants, displaying 97.4% similarity with StFDH, 95.8% with SmFDH and 95.3% with CaFDH, while showing 81.4% and 78.7% similarity with AtFDH and VuFDH, respectively. Notably, the signal peptide of SlFDH shares the highest similarity with that of StFDH, which displays two site differences located at the fourth and 15th amino acid positions, respectively (Figure S1). Furthermore, the sites for catalytic activity and NAD$^+$-binding are highly conserved among these FDHs. In addition, the sites for formate binding and nucleotide binding are conserved among these six FDH proteins, with only a Leu replaced by Pro in SlFDH and an Ile being replaced by Thr in AtFDH.

SlFDH localizes to mitochondria

Sequence analysis by Plant-mPLoc (http://www.csbio.sjtu.edu.cn/cgi-bin/PlantmPLoc.cgi) predicted that SlFDH is a mitochondrion-localized protein (Figure S2a). Predotar
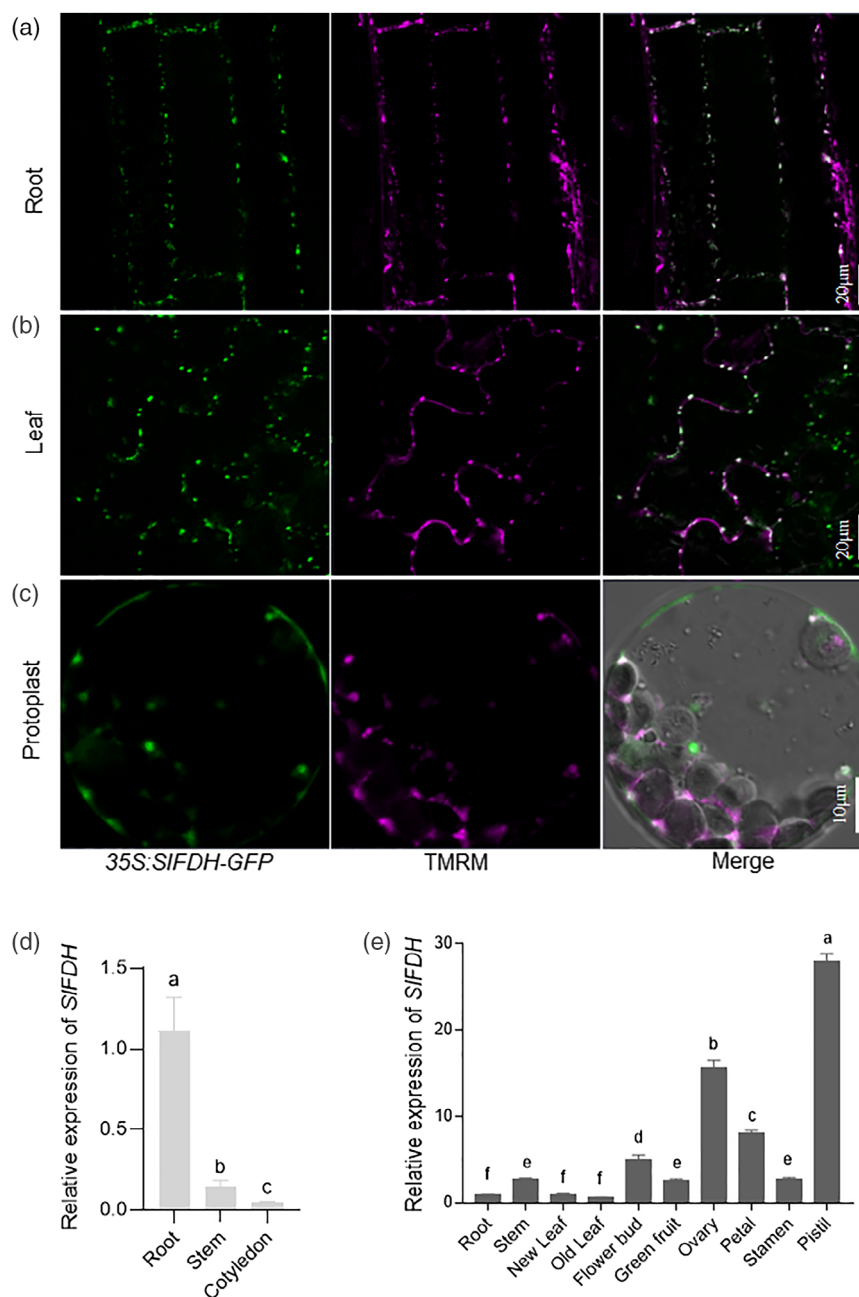
Figure 1. Subcellular localization of SlFDH, and tissue-specific expression of *SlFDH*.
(a–c) Confocal laser-scanning microscopy of SlFDH-GFP fusion protein in transgenic Arabidopsis plants expressing *35S:SlFDH-GFP*. Signals were observed in (a) roots, (b) leaves and (c) protoplasts. Tetramethyl rhodamine methyl ester (TMRM) was used as a mitochondrial marker. Scale bars: 20 μm.
(d) Reverse transcription-quantitative polymerase chain reaction (RT-qPCR) analysis of *SlFDH* expression at the seedling stage (7 days old).
(e) RT-qPCR analysis of *SlFDH* expression at the reproductive stage (70 days old). Data are means ± SD ($n = 3$). Different letters indicate significant differences by two-way ANOVA with Tukey's multiple comparison test ($P < 0.05$).

(Small et al., 2004) predicted that SlFDH contains a 34-amino acid cleavable N-terminal signal peptide with a 99.7% probability of export to mitochondria (Figure S2b). To assess the localization of SlFDH, we generated transgenic Arabidopsis lines by introducing a construct encoding an SlFDH-GFP (green fluorescent protein) fusion protein under the control of the cauliflower mosaic virus

(CaMV) 35S promoter. We detected punctiform green fluorescent signals in both the roots and leaves of *35S:SlFDH-GFP* transgenic plants, which coincided with the staining of the mitochondrion-specific fluorescent dye tetramethyl rhodamine methyl ester (TMRM; Figure 1a,b). We isolated protoplasts from the leaves of the transgenic plants and confirmed that the SlFDH-GFP fusion protein localizes to
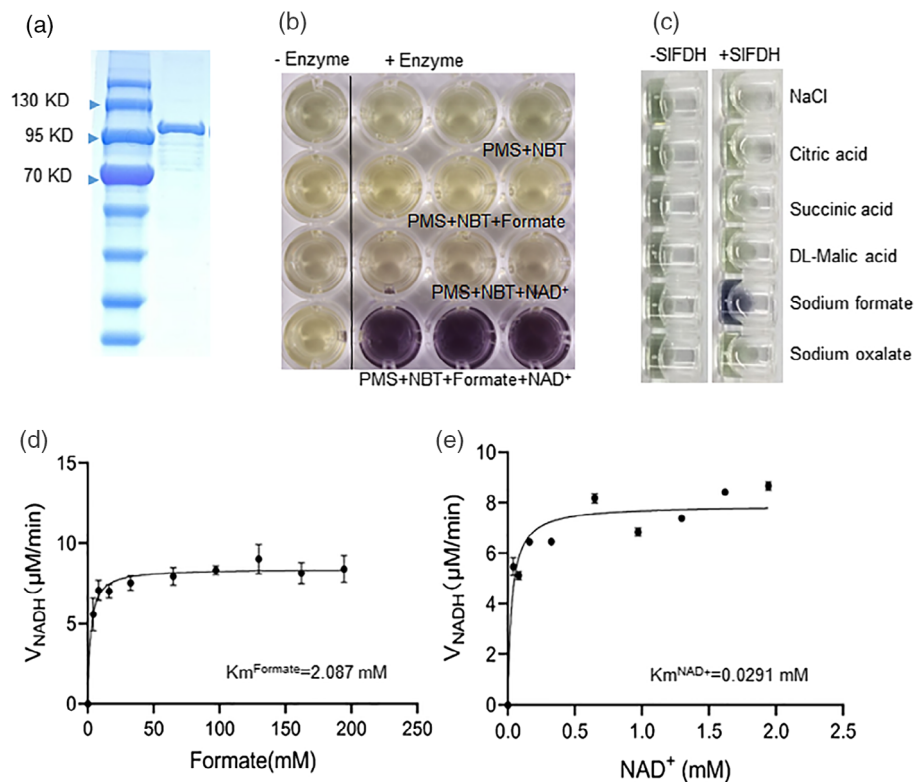
Figure 2. Biochemical analysis of recombinant SlFDH protein.

(a) Sodium dodecyl sulfate–polyacrylamide gel electrophoresis of purified SlFDH protein.

(b) Chromogenic reaction of SlFDH-formate with nitroblue tetrazolium (NBT) and phenazine methosulfate (PMS). The reaction mixture contained 2 µg recombinant SlFDH protein, 0.4 mм NAD^+, 0.003 mg ml^{-1} PMS and 0.4 mg ml^{-1} NBT at pH 7.5. The production of a blue-purple color suggests the catalytic activity of SlFDH towards formate, resulting in the production of NADH for the coupled reaction to produce formazan.

(c) Substrate specificity of SlFDH. Formate dehydrogenase (FDH) activity was examined at pH 7.5 with various substrates: citric acid, succinic acid, DL-malic acid, sodium formate and sodium oxalate at a concentration of 50 mм. NaCl was used as a control.

(d, e) Kinetic analysis of SlFDH using a range of formate and NAD^+ concentrations as indicated, respectively. Data are means ± SD ($n = 3$).

mitochondria, and the signals did not overlap with the autofluorescence of chloroplasts (Figure 1c).

SlFDH shows high sequence similarity with StFDH (Figure S1). StFDH (Ambard-Bretteville et al., 2003a), CaFDH (Choi et al., 2014) and VuFDH (Lou, Gong, et al., 2016) are mitochondria-localized proteins, although AtFDH was detected in both mitochondria and chloroplasts (Herman et al., 2002). These findings suggest that FDH proteins in Solanaceae are localized to mitochondria and that they might share conserved functions.

We used reverse transcription-quantitative polymerase chain reaction (RT-qPCR) to compare the expression levels of *SlFDH* in different organs and tissues. In 1-week-old seedlings, the expression level of *SlFDH* was higher in roots than in stems and cotyledons (Figure 1d). By contrast, at the reproductive stage (70-day-old plants), *SlFDH* was expressed at high levels in ovary, pistil and petal tissue, but at relatively low levels in vegetative organs such as leaves, stems and roots (Figure 1e), likely because the vegetative organs had begun to senesce.

SlFDH is a FDH

Sequence alignment strongly suggested that the protein encoded by *SlFDH* is an NAD-dependent enzyme (Figure S1). To characterize its biochemical function, we purified recombinant SlFDH protein produced in *Escherichia coli* upon induction with isopropyl β-D-1-thiogalactopyranoside (IPTG; Figure 2a; Figure S3). We measured FDH activity by monitoring the production of blue-purple formazan produced via the reaction of phenazine methosulfate (PMS) with NADH derived from the catalysis of formate and NAD^+. Indeed, we detected formazan in the presence of recombinant SlFDH, indicating that the protein does exhibit FDH activity (Figure 2b).

To determine the substrate specificity of SlFDH, we assayed the activity of SlFDH with other organic acids. We thus tested the potential substrates DL-malic acid, citric acid, sodium formate, succinic acid and sodium oxalate, using 50 mм NaCl at pH 7.0 as the negative control. The addition of high concentrations of some substrates prevented color formation, such as 162 mм DL-malic acid or

citric acid. However, formate concentrations as high as 162 mM had no effect on color formation (Figure S4a). Having confirmed that formate would not interfere with the reaction, we analyzed the chemical reactions of SlFDH with different substrates. The blue-purple color was produced only when formate was present in the reaction (Figure 2c), indicating that SlFDH specifically degrades formate.

We also performed steady-state kinetic experiments using a range of formate and NAD^+ concentrations. Based on enzymatic kinetics, we calculated the K_m values as $K_m^{formate} = 2.087$ mM and $K_m^{NAD^+} = 29.1$ μM (Figure 2d,e), which are comparable to those of other FDHs, such as birdsfoot trefoil (*Lotus japonicus*) LjFDH1 (Andreadeli et al., 2009). Together, these results indicate that SlFDH is a FDH that catabolizes formate into CO_2 and reduces NAD^+ to NADH.

Expression pattern of *SlFDH* in response to Al stress

The expression of FDH genes in plants is responsive to various biotic and abiotic stresses. We previously demonstrated that the expression of *VuFDH* was induced by Al stress in rice bean; introducing *VuFDH* into tobacco increased plant tolerance to Al and low pH (Lou, Gong, et al., 2016). In addition to degradation by FDH, formate is readily incorporated into one-carbon metabolism pathways (Hanson & Roje, 2001). For instance, ^{13}C-NMR (nuclear magnetic resonance) analysis demonstrated a substantial flux from supplied formate to serine in Arabidopsis (Prabhu et al., 1996). Under drought stress, formate accumulation was not observed in transgenic potato plants with no detectable FDH activity, but a transient increase in formate levels was detected in untransformed plants, pointing to metabolic bypass to compensate for the absence of FDH activity (Ambard-Bretteville et al., 2003b). Therefore, it remains unclear whether loss-of-function mutations of *FDH* contribute to Al sensitivity. Moreover, the promoter activity of *AtFDH* was not affected by Al stress (Figure S5), which is in agreement with the finding that *AtFDH* expression is not regulated by Al stress (Sawaki et al., 2009). Therefore, it appears that the responsiveness of FDH depends not only on the stress imposed on plants but also on the plant species.

To examine whether *SlFDH* is responsive to Al stress, we exposed 1-week-old tomato (cv. Micro-Tom) seedlings to 10 μM Al for 6 h. *SlFDH* was upregulated approximately fivefold in root tips (0–1 cm), while it was not significantly induced by Al in the 1–2-cm region of the root (Figure 3a). The expression level of *SlFDH* increased with increasing Al concentration (Figure 3b). Compared with 6 h of exposure, the induction of *SlFDH* expression was less obvious in response to 24 h of Al exposure, but it did remain upregulated (Figure 3c). To examine the specificity of *SlFDH* induction, we monitored the expression of *SlFDH* in response to different heavy metals such as Al^{3+}, copper

(Cu^{2+}), Cd^{2+} and lanthanum (La^{3+}). *SlFDH* was significantly induced by Al treatment, slightly induced by Cu^{2+}, but not induced by Cd^{2+} or La^{3+} treatment. The expression of *SlFDH* was not affected by exposing the roots to different pH levels (Figure 3d).

SlFDH loss-of-function mutants are sensitive to Al stress

To examine the role of SlFDH in Al tolerance, we generated *Slfdh* mutants in the Micro-Tom background by CRISPR/Cas9 genome editing. We obtained two mutant lines: one mutant (named *Slfdh-1*) had a 1-bp deletion in both the first and second targets; and the other (named *Slfdh-2*) had a 1-bp deletion in the first target (Figure 4a, b). We compared Al sensitivity between WT seedlings and the two mutants. We first examined the root growth response of WT seedlings to different concentrations of Al for different treatment durations. After 1 day of treatment, we observed a significant inhibition of root growth only in response to 15 μM Al at pH 5.0. After 2 days of treatment, 10 μM Al (pH 5.0) significantly inhibited root elongation as well. However, 5 μM Al had no significant effect on root elongation in WT plants after 3 days of treatment (Figure S6).

Given that FDH plays a positive role in Al tolerance in plants (Lou, Gong, et al., 2016), we reasoned that the loss-of-function of *SlFDH* would result in increased Al sensitivity. Therefore, we chose an Al concentration of 10 μM to compare the Al sensitivity between WT and *Slfdh* mutants. In the absence of Al, root elongation did not differ between WT and *Slfdh*. However, root elongation was significantly inhibited in *Slfdh-1* and *Slfdh-2* relative to WT seedlings in response to 24 h of 10 μM Al treatment (Figure 4c,d), indicating that an FDH-dependent metabolic pathway helps alleviate Al toxicity in the tomato root apex. We then examined cell death in the root apex in response to Al stress using Evans blue staining (Yamamoto et al., 2001). The uptake of Evans blue (a cell membrane non-permeable dye) was greater in both *Slfdh* mutants than WT seedlings (Figure 4e), suggesting that the plasma membrane was more severely damaged in *Slfdh* than in WT seedlings exposed to Al stress.

Analyzing the sensitivity of tomato to formate

To explore the underlying mechanism of SlFDH-mediated Al tolerance, we examined the sensitivity of tomato seedlings to exogenous formate treatment at various concentrations. A formate concentration of 0.3 mM has no effect on tomato root elongation after 3 days of treatment. However, formate levels as high as 0.6 mM significantly inhibited root elongation after 1 day of treatment, and this inhibition became more severe over time (Figure 5a), suggesting that formate accumulation might be detrimental to root elongation. We also compared the sensitivity of roots to formate in WT seedlings and the two *Slfdh* mutants.
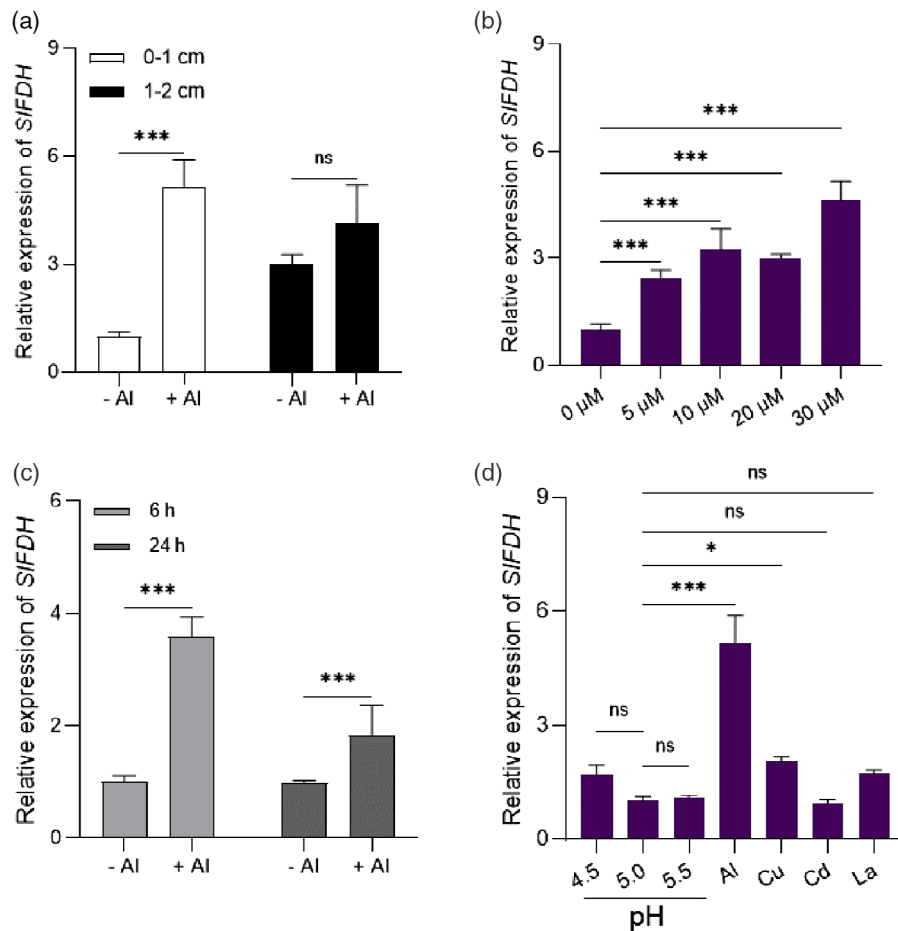
Figure 3. Expression analysis of *SlFDH*.

(a) Relative expression of *SlFDH* in root tips (0–1 cm) and basal roots (1–2 cm) after 6 h of 10 μM Al treatment.

(b) Dose-dependent *SlFDH* expression in tomato root tips (0–1 cm) treated with different concentrations of Al for 6 h.

(c) Time-dependent expression of *SlFDH* under Al stress. One-week-old seedlings were treated with or without 10 μM Al (pH 5.0, 1/5 Hoagland with 10 μM $NH_4H_2PO_4$) for 6 and 24 h, and root tips (0–1 cm) were excised for RNA extraction.

(d) Specificity of *SlFDH* expression. One-week-old seedlings were exposed to different pH levels and various metals for 6 h, and root tips (0–1 cm) were excised for RNA extraction. The expression level of *SlFDH* was measured by reverse transcription-quantitative polymerase chain reaction (RT-qPCR), and *SlGAPDH* was used as an internal control. Values are means ± SD ($n = 6$). Statistical analysis was performed by Student's *t*-test (ns, not significant; *$P < 0.05$, ***$P < 0.001$).

Compared with WT, both *Slfdh-1* and *Slfdh-2* displayed more severe inhibition of root elongation in response to 0.6 mM formate treatment (Figure 5b), suggesting that SlFDH can degrade formate *in planta*.

Because formate accumulation is detrimental to root elongation and SlFDH contributes to formate degradation, we wondered whether formate accumulation contributes to Al-induced inhibited root elongation in tomato. We initially tried to analyze changes in formate content in both WT and mutants seedlings. However, we failed to detect changes in formate concentrations in response to Al stress, likely due to the extremely low concentrations of formate in root tips.

We then investigated whether Al-induced *SlFDH* expression is dependent on formate by analyzing *SlFDH* expression in response to exogenous formate. Unexpectedly, when we exposed tomato roots to 0.6 mM formate for 6, 12 or 24 h, *SlFDH* expression was not induced. In fact, *SlFDH* expression was repressed by 24 h of formate treatment (Figure 5c). These results indicate that *SlFDH* expression is not induced by formate, which is consistent with the finding for *AtFDH* (Fukusaki et al., 2000). Finally, as an alternative, we analyzed Al-induced NAD^+ accumulation in tomato root tips. We performed a WST-8 assay using a water-soluble tetrazolium salt that offers a sensitive and rapid method for detecting NADH (Figure 6a). NAD_{total} (NAD^+ and NADH) accumulation in tomato roots dramatically increased in response to Al stress; however, NADH was not significantly affected by this treatment (Figure 6b,c). These results suggest that NAD^+ rather than formate is responsible for the induction of *SlFDH* expression under Al stress.
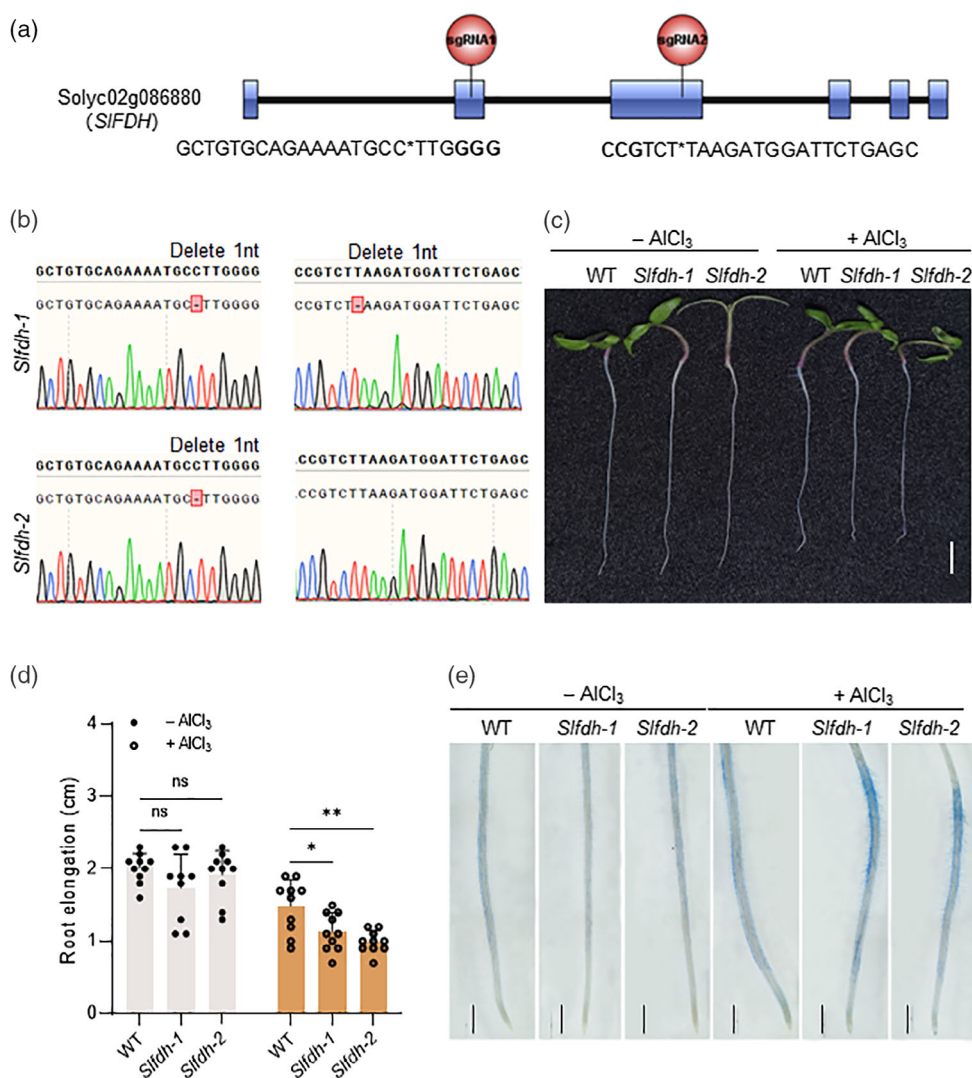
Figure 4. Loss-of-function mutants of *SlFDH* show increased sensitivity to Al.

(a) Schematic diagram of the pair of sgRNA target sites in Solyc02g086880 (*SlFDH*).

(b) CRISPR-generated *Slfdh-1* and *Slfdh-2* alleles were identified from T0 mutant events; *Slfdh-1* contains a 1-bp deletion in both targets, and *Slfdh-2* contains only a 1-bp deletion in the first target. Allele sequences were determined by DNA sequencing.

(c) Representative 7-day-old wild-type (WT) and *Slfdh* seedlings with or without 10 μM Al (pH 5.0, 1/5 Hoagland with 10 μM $NH_4H_2PO_4$) treatment for 24 h; scale bars: 1 cm.

(d) Root elongation of WT and *Slfdh-1* and *Slfdh-2* homozygous lines with or without 10 μM Al treatment for 24 h. Values are means $\pm$ SD ($n > 10$). Statistical analysis was performed by Student's *t*-test (ns, not significant; *$P < 0.05$, **$P < 0.01$).

(e) Evans blue staining of 7-day-old WT and *Slfdh* seedings with or with Al treatment as described above. After Evans blue staining, the seedings were observed under a Nikon AZ100 microscope; scale bars: 1 mm.

Transcriptional regulation of *SlFDH* in tomato

To discover components involved in regulating *SlFDH* expression, we constructed gene regulatory networks centered on *SlFDH* using the TomExpress co-expression tool (Zouine et al., 2017). We identified 18 genes co-expressed with *SlFDH* at the conservative threshold of correlation values greater than 0.6 (Table S1). Among these, six genes were annotated as TF genes, suggesting that they might regulate *SlFDH* expression (Figure 7a). To test this notion, we performed a dual-luciferase reporter assay using the

firefly luciferase (*LUC*) reporter gene driven by a 2088-bp *SlFDH* promoter fragment as the reporter and the *Renilla* luciferase (*REN*) gene driven by the 35S promoter (Figure S7a). Of these six TFs, SlSEP1, LeMYB1 and MADS-box protein 5 (SlMBP5) activated the *proSlFDH:LUC* reporter construct in *Nicotiana benthamiana* leaves (Figure S7b), especially SlSEP1 and SlMBP5, whereas the others (ERF008, SlMBP9 and ERF110) did not (Figure S7c). To further investigate whether these TF genes regulate *SlFDH* expression in tomato root tips in response to Al, we
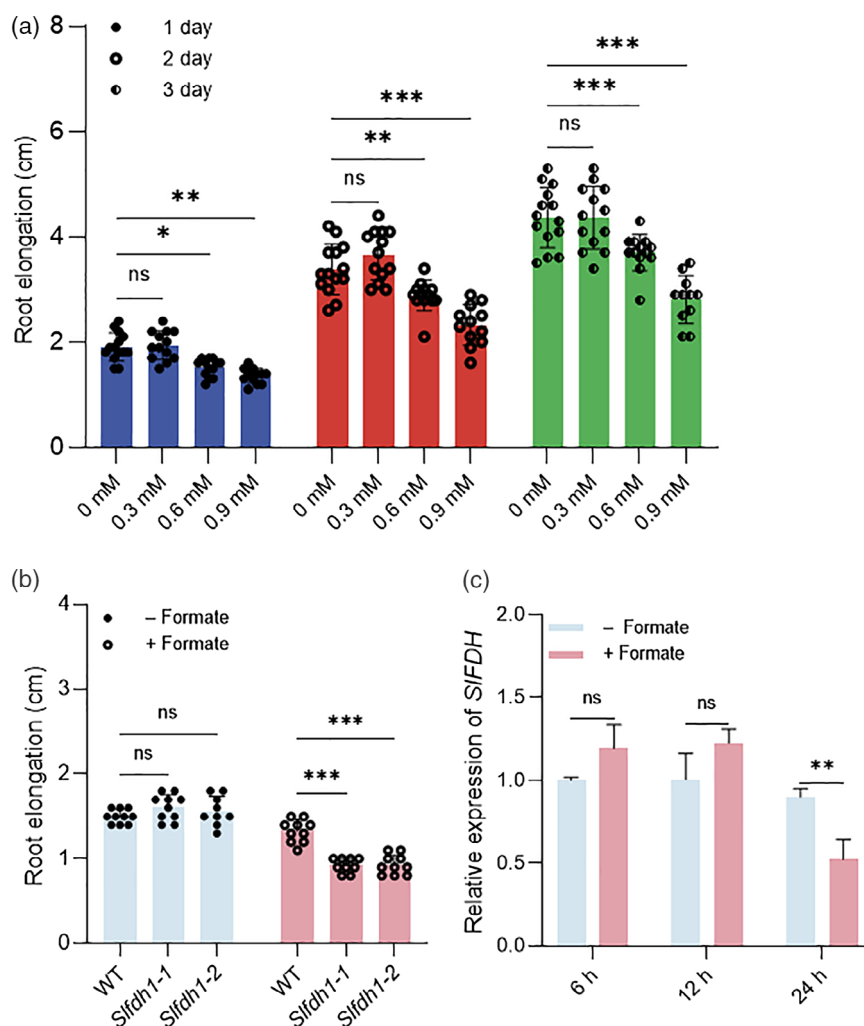
Figure 5. Analysis of the sensitivity of tomato to formate treatment.

(a) Root elongation of Micro-Tom tomato treated with different concentrations of formate. One-week-old wild-type (WT) seedlings were transferred from 1/5 Hoagland solid medium to 1/5 Hoagland nutrient solution containing 0, 0.3, 0.6 or 0.9 mM formate (pH 5.0). Root length was measured after 1, 2 and 3 days. Values are means ± SD ($n \geq 10$).

(b) Root elongation in WT, *Slfdh-1* and *Slfdh-2* seedlings with or without 0.6 mM formate treatment for 24 h. Root length was measured with a ruler before and after treatment. Values are means ± SD ($n = 10$).

(c) Relative expression of *SlFDH* in roots after 0.6 mM formate treatment for 6, 12 or 24 h (pH 5.0, 1/5 Hoagland). Data are means ± SD ($n = 3$). Statistical analysis was performed by Student's *t*-test (ns, not significant; *$P < 0.05$, **$P < 0.01$, ***$P < 0.001$).

analyzed their expression based on our previously generated transcriptome data from tomato root apex tissue under Al stress (Jin et al., 2020). However, all six TF genes were expressed at extremely low levels in root tips, and their expression was not significantly affected by Al (Figure 7b), suggesting that these TFs are not involved in Al-induced *SlFDH* expression in root tips.

Arabidopsis SENSITIVE TO PROTON RHIZOTOXICITY 1 (STOP1) and its homologs in other plants, such as ALUMINUM RESISTANCE TRANSCRIPTION FACTOR 1 (ART1) in rice and SlSTOP1 in tomato, are master TFs that induce the expression of Al-tolerance genes (Iuchi et al., 2007;

Zhang et al., 2022). We therefore reasoned that SlSTOP1 is likely responsible for the induction of *SlFDH* expression under Al stress. However, the protein level but not mRNA level of Arabidopsis STOP1 is influenced by Al (Iuchi et al., 2007; Zhang et al., 2019). Two homologs of Arabidopsis *STOP1* are present in the tomato genome: *SlSTOP1* and *SlSTOP2*. Transcriptome analysis revealed that the expression levels of *SlSTOP1* and *SlSTOP2* were not influenced by Al in the tomato root apex (Jin et al., 2022). Therefore, it was not possible to identify SlSTOP1 or SlSTOP2 as a candidate regulator of *SlFDH* based on gene regulation networks. Thus, we examined
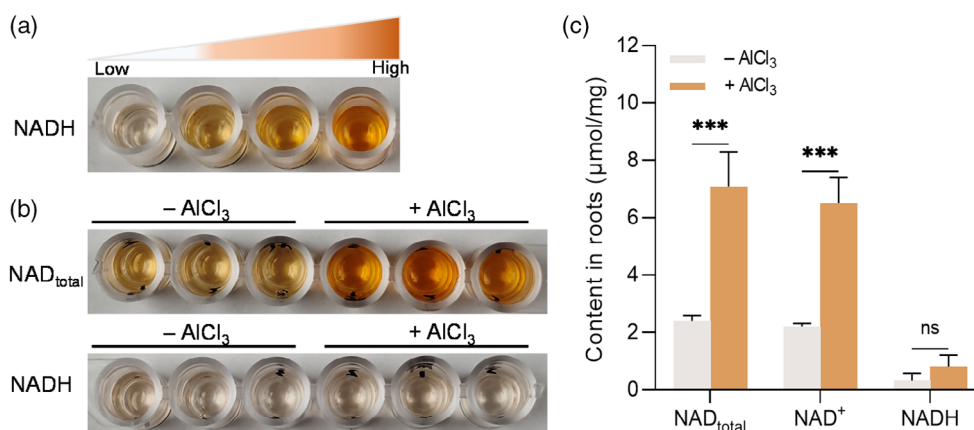
Figure 6. Al-induced NAD^+ accumulation in tomato root tips.

(a) WST-8 assay of NADH based on a chromogenic reaction; color formation is dependent on the NADH concentration in the solution.

(b) Chromogenic reaction of NAD_{total} (NAD^+ + NADH) and NADH in tomato root tips. One-week-old seedlings were treated with or without 10 μM $AlCl_3$ for 24 h, and root tips were excised. Upper panel shows NAD_{total}, and lower panel shows NADH only in extraction solution from tomato root tips obtained by incubating the solution at 60°C to decompose NAD^+.

(c) NAD_{total}, NAD^+ and NADH contents in roots with or without $AlCl_3$ treatment. Data are means ± SD (n = 3). Statistical analysis was performed by Student's *t*-test (ns, not significant; ***P < 0.001).

the possibility that *SlFDH* is regulated by SISTOP1 or SISTOP2 using PlantRegMap (Tian et al., 2020). We searched a 2000-bp promoter fragment of *SlFDH* in PlantRegMap (http://plantregmap.gao-lab.org/binding_site_prediction_result.php), and identified a potential binding site for SISTOP1 that resides between 1152 and 1138 bp upstream from the ATG (Figure 7d).

To determine whether SISTOP1 and/or SISTOP2 regulate *SlFDH* expression, we performed a dual-luciferase reporter assay using the *LUC* gene driven by the 2088-bp *SlFDH* promoter and the *REN* gene driven by the 35S promoter. SISTOP1 but not SISTOP2 activated the *ProSlFDH:LUC* reporter gene when transiently co-expressed in *N. benthamiana* leaves (Figure 7c). We then generated *Slstop1* and *Slstop2* mutants via CRISPR/Cas9 genome editing. *Slstop1-1* and *Slstop1-2* contain a 148-bp deletion between the two target sites and a 48-bp deletion near the sgRNA1 site, respectively (Figure S8), while *Slstop2-1* and *Slstop2-2* harbor a 156-bp deletion between the two target sites and a 1-bp deletion in target 2, respectively (Figure S9a,b). We compared the transcriptional levels of *SlFDH* between WT, *Slstop1* and *Slstop2* with or without Al treatment. Whereas Al significantly induced the expression of *SlFDH* in WT and *Slstop2* plants (Figure 7f; Figure S9c), the expression of this gene was not affected by Al in the *Slstop1* mutants (Figure 7f), indicating that Al-induced expression of *SlFDH* is dependent on SISTOP1. Finally, in an electrophoretic mobility shift assay (EMSA), SISTOP1 bound to the *SlFDH* promoter, and this binding activity was reduced by adding unlabeled competitor (Figure 7e). Importantly, the mutated *cis*-element failed to interact with SISTOP1 in the EMSA (Figure 7e).

© 2022 Society for Experimental Biology and John Wiley & Sons Ltd.,
The Plant Journal, (2023), **113**, 387–401

DISCUSSION

SlFDH catalyzes formate degradation and NAD^+ reduction

In this present study, we identified the FDH gene *SlFDH* in tomato. SlFDH showed catalytic specificity to formate among various substrates (Figure 2c), which is consistent with the finding that FDH proteins from plants contain typical NAD^+ binding and formate binding domains (Figure S1). Our FDH activity assay also supported the finding that FDH catalyzes the conversion of formate to CO_2 coupled with the reduction of NAD^+ to NADH, as blue-purple color formation in the assay depends on the reduction of PMS by NADH. Analysis of the kinetic properties of recombinant SlFDH showed that the calculated $K_m^{formate}$ was 2.087 mM and $K_m^{NAD^+}$ was 29.1 μM, which are comparable to the values reported for *L. japonicus* LjFDH1 ($K_m^{formate}$ is 6.1 mM, and $K_m^{NAD^+}$ is 25.9 μM; Andreadeli et al., 2009). K_m values of 1.6 mM for formate and 72 μM for NAD^+ have been reported for mung bean (*Phaseolus aureus*; Peacock & Boulter, 1970), and K_m values of 0.6 mM and 57 μM, respectively, for *G. soja* (Farinelli et al., 1983). The K_m value of FDH in extracts of spinach (*Spinacia oleracea* L.) leaves was estimated to be 1.7 mM. Similar K_m values were also reported for bacterial FDH (Halliwell, 1974). For example, in *Ancylobacter aquaticus* strain KNK607M, the K_m values for formate and NAD^+ are 2.4 mM and 57 μM, respectively (Nanba et al., 2003). In *Paracoccus* sp. strain 12-A, the K_m values for formate and NAD^+ were calculated to be 5.0 mM and 36 μM, respectively (Iida et al., 1992). However, different substrate affinities have been reported for FDH in Arabidopsis leaves. For instance, Li et al. (2000) purified FDH from leaf mitochondria and determined that the K_m values
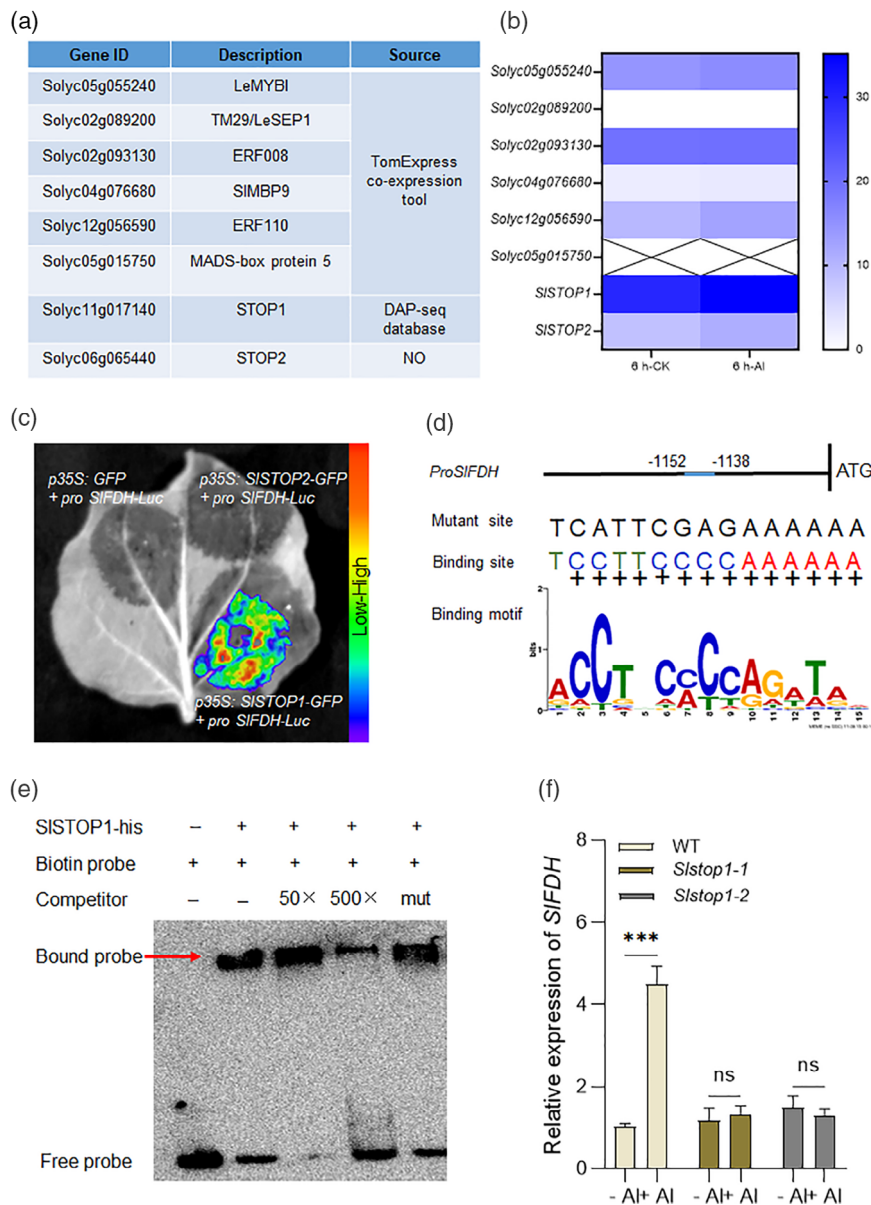
Figure 7. Analysis of the transcriptional regulation of *SlFDH* in tomato.
(a) Putative transcription factors (TFs) identified by co-expression matrix (correlation coefficient > 0.6) analysis according to gene expression data from TomExpress or PlantRegMap (http://plantregmap.gao-lab.org/binding_site_prediction_result.php).
(b) Expression levels of all eight TF genes with or without 6 h Al treatment; data were derived from our previously generated transcriptome data (Jin et al., 2020). Color scale represents FPKM values (indicating transcript abundance).
(c) Dual-luciferase assays in *Nicotiana benthamiana* leaves. *Nicotiana benthamiana* leaves were co-infiltrated with empty vector (*p35S:GFP*) or TF (*SlSTOP1* or *SlSTOP2*)-containing effector and the *proSlFDH:LUC* reporter.
(d) The predicted STOP1 binding motif in the DAP-seq database. The binding site (blue line) derived from *ProSlFDH* used in the electrophoretic mobility shift assay (EMSA).
(e) Binding of recombinant His-SlSTOP1 to the predicted binding site of *ProSlFDH*. The biotin-labeled fragment was incubated with 2 μg recombinant purified SlSTOP1 protein. A 50- or 500-fold excess of unlabeled probe and 500-unlabeled mutant probe were added as a competitor. The red arrow indicates the positions of protein–DNA complexes.
(f) *SlFDH* expression in wild-type (WT), *Slstop1-1* and *Slstop1-2* seedlings with or without 6 h of Al treatment. 7-day-old WT, *Slstop1-1* and *Slstop1-2* seedings were treated with or without 10 μM for 6 h. *SlGAPDH* was used as the internal control. Values are means ± SD (n = 6). Statistical analysis was performed by one-way ANOVA (ns, not significant; ***P < 0.001).

were 1.4 mm for formate and 34 μm for NAD$^+$, respectively. By contrast, higher K_m values for FDH substrates (10 mm and 65 μm for formate and NAD$^+$, respectively) were

reported by Olson et al. (2000). These differences could be attributed to factors such as heating during purification, as the protein may refold into a second form with altered

kinetic constants under this treatment (Baack et al., 2003). Therefore, the induction of *SlFDH* expression under Al stress is likely associated with formate degradation and NADH production.

SlFDH positively affects Al tolerance

Formate dehydrogenase has been implicated in stress tolerance in various plants. For instance, potato plants expressing an antisense *FDH* gene exhibited higher formate accumulation in both leaves and tubers compared with WT plants (Ambard-Bretteville et al., 2003b). Overexpressing *AtFDH* increased the tolerance of transgenic Arabidopsis to high concentrations of formate but not methanol or formaldehyde (Li et al., 2002). Overexpressing *AtFDH* driven by the promoter of the Rubisco small subunit gene in chloroplasts increased formaldehyde uptake and metabolism in tobacco leaves (Wang et al., 2018). However, few studies have focused on the functional characterization of FDH in plants in response to stress. The rice bean gene *VuFDH* functions in Al tolerance, as revealed in transgenic tobacco plants (Lou, Gong, et al., 2016), but the effect of its loss-of-function on Al stress is unknown. In the present study, we demonstrated that SlFDH functions in Al tolerance in tomato. This conclusion is based on the following lines of evidence. First, the expression of *SlFDH* was dramatically induced by Al but little affected by other metals (Figure 3d), and this induction was confined to the root apex, the primary site of Al toxicity (Yang et al., 2019). Second, *Slfdh* mutants exhibited increased sensitivity to Al stress compared with WT plants (Figure 4c–e).

SlSTOP1 positively regulates *SlFDH* expression under Al stress

Despite numerous reports on the induction of *FDH* genes under various stresses, little is known about how the expression of *FDH* is regulated by stress. Here, by performing co-expression and correlation network analyses, we identified six TFs as potential transcriptional regulators of *SlFDH* expression (Figure 7a), but only SlSEP1 and SlMBP5 indeed regulate *FDH* expression. Although these two TF genes are expressed at low levels in the root apex (leading to a failure to detect their expression in roots with or without Al treatment; Figure 7b), these genes are highly expressed in other organs such as fruits (https://tea.sgn.cornell.edu/), indicating that the encoding TFs might play tissue-specific roles in regulating *SlFDH* expression; such roles remain to be investigated. The finding that *SlFDH* is highly expressed in reproductive organs also supports this notion (Figure 1e).

The induction of *SlFDH* depended on SlSTOP1 but not SlSTOP2 (Figure 7f; Figure S9). The finding that SlSTOP2 does not regulate *SlFDH* expression is not unexpected, even though this protein is homologous to SlSTOP1. Similar results have been reported in other plants. For instance,

rice ART2, an ART1 homolog, contributes to Al tolerance by regulating the expression of genes not regulated by ART1 (Che et al., 2018). AtSTOP2 only moderately complemented the role of AtSTOP1 in regulating the expression of Al tolerance genes (Kobayashi et al., 2014). Here, EMSA confirmed that SlSTOP1 directly binds to the promoter of *SlFDH* (Figure 7e). SlSTOP1 is homologous to AtSTOP1, which functions as a master TF that controls Al tolerance by directly regulating the expression of many Al tolerance genes. Thus, the direct regulation of *SlFDH* by SlSTOP1 provides another layer of evidence that *SlFDH* is an important gene in Al tolerance. However, it is worth noting that the transcriptional regulation of *FDH* genes differs among plant species. For instance, *FDH* was induced by formate treatment in rice (Shiraishi et al., 2000), but not in Arabidopsis (Fukusaki et al., 2000). In the current study, in a *AtFDHpro::GUS* (ß-glucuronidase) activity assay (Figure S5), *AtFDH* transcription was not responsive to Al stress in Arabidopsis, which is in agreement with a previous report (Sawaki et al., 2009). Therefore, AtSTOP1 might be necessary but not sufficient for the transcriptional induction of *AtFDH*.

SlFDH provides an alternative pathway to produce NADH under Al stress

Unexpectedly, we found that formate did not induce the expression of *SlFDH* in the tomato root apex (Figure 5c). Al-induced formate accumulation was previously observed in the root apex in rice bean and tobacco (Lou, Gong, et al., 2016). However, we failed to observe any changes in formate levels in the tomato root apex in response to Al stress, indicating that formate might not be responsible for the induction of *SlFDH*. This observation raises two basic questions: how is *SlFDH* induced by Al stress; and what is the role of *SlFDH* induction in Al stress tolerance in the tomato root apex, as formate does not accumulate in this tissue?

Regarding the induction of *SlFDH* by Al stress, a previous study proposed that glycolysis plays an important role in *FDH* expression in response to abiotic stress (Hourton-Cabassa et al., 1998). Similarly, we previously demonstrated that Al stress represses the expression of genes involved in glycolysis and induces genes related to anaerobic respiration in the root apex of rice bean (Fan et al., 2014). Hypoxia has also been implicated in iron deficiency-induced *FDH* expression in barley roots (Suzuki et al., 1998). These findings suggest that hypoxia and glycolysis may contribute to *FDH* expression in response to Al stress.

Regarding the role of *SlFDH* induction in Al stress, perhaps the accumulation of SlFDH is favorable for the production of NADH, which produces extra ATP via the respiratory electron chain for various biological processes, provides a reducing reagent for biochemical reactions, and

scavenges reactive oxygen species produced in response to Al stress (Figure S10). In support of this notion, FDH helps supply energy for methylotrophic microorganisms (Tishkov & Popov, 2004), and NAD$^+$ dramatically accumulated in tomato roots after Al treatment (Figure 6). Moreover, Al-induced lipid peroxidation was aggravated in the *Slfdh* mutants compared with WT plants (Figure 4e). The finding that SlFDH localizes to the mitochondria also supports this viewpoint (Figure 1a). Considering that Al stress exerts its toxicity at multiple cellular levels and targets various components (Zheng & Yang, 2005), it is possible that plant cells require a vast amount of energy to adapt to Al stress. Therefore, FDH-mediated NADH production in mitochondria provides an alternate way to supply energy to plants under Al stress (Figure S10). From this perspective, it is reasonable to speculate that NAD$^+$ accumulation might trigger SlSTOP1 to regulate *SlFDH* expression.

In summary, we characterized the SlFDH protein in tomato, including its catalytic kinetics, role in Al tolerance and activity in regulating gene expression. SlFDH showed high substrate specificity to both formate and NAD$^+$, with a much higher affinity for NAD$^+$ than formate. Furthermore, loss-of-function mutants of *SlFDH* displayed increased sensitivity to Al stress. Finally, we identified several TFs that play important roles in regulating *SlFDH* expression, especially SlSTOP1, which regulates Al-induced *SlFDH* expression.

EXPERIMENTAL PROCEDURES

Plant materials, growth conditions and treatments

All tomato plants used in this study were in the Micro-Tom background. To generate CRISPR/Cas9 gene editing knockout mutants, two targets (Table S2) were designed (http://crispr.hzau.edu.cn/cgi-bin/CRISPR2/CRISPR) for each gene, fused into a CRISPR vector (BGK012; BIOGLE GeneTech, Hangzhou, China), and introduced into tomato plants via Agrobacterium (*Agrobacterium tumefaciens*)-mediated transformation (Dan et al., 2006). Mutations were identified by PCR and sequencing. All possible off-target sites predicted in CRISPR 2.0 (http://crispr.hzau.edu.cn/cgi-bin/CRISPR2/CRISPR) were analyzed by PCR and sequencing.

Seeds were soaked in 10% (w/v) NaClO$_3$ for 15 min, washed three times with sterile ddH$_2$O, and incubated at 37°C for 2 days in the dark for stratification. The seeds were sown in 1/5 Hoagland medium comprising 0.4 mM MgSO$_4$, 0.2 mM NH$_4$H$_2$PO$_4$, 1 mM KNO$_3$, 1 mM Ca(NO$_3$)$_2$, 20 μM Fe-EDTA, 3 μM H$_3$BO$_3$, 0.5 μM MnCl$_2$, 0.2 μM CuSO$_4$, 0.4 μM ZnSO$_4$, (NH$_3$)$_6$Mo$_7$O$_2$ (Hoagland & Arnon, 1950) and 0.8% (w/v) agar, and transferred to a growth chamber at 23°C under a 16-h light/8-h dark photoperiod. After 5 days, uniform seedlings were exposed to the following treatments. For the time experiments, seedlings were treated with or without 10 μM Al (pH 5.0, 1/5 Hoagland with 10 μM NH$_4$H$_2$PO$_4$) for 6 or 24 h. For the Al dose experiment, seedlings were treated with various concentrations of Al (0, 5, 10, 20 or 30 μM, pH 5.0, 1/5 Hoagland with 10 μM NH$_4$H$_2$PO$_4$) for 6 h. For the pH and other metal experiments, seedlings were exposed to different pH levels (1/5 Hoagland with 10 μM NH$_4$H$_2$PO$_4$) or metal treatments (10 μM AlCl$_3$, 20 μM CdCl$_2$, 10 μM LaCl$_3$ or 0.5 μM CuCl$_2$; pH 5.0, 1/5 Hoagland with 10 μM

NH$_4$H$_2$PO$_4$) for 6 h. For exogenous formate treatment, seedlings were treated with 1/5 Hoagland medium (pH 5.0) with various concentrations of formate. *SlGAPDH* was used as an internal control. Root length was measured with a ruler, and root elongation was calculated before and after treatment (Jin et al., 2020).

Cloning of *SlFDH*, purification of recombinant SlFDH protein and biochemical analysis of SlFDH

The cDNA sequence of *SlFDH* was identified by BLAST in Phytozome (https://phytozome-next.jgi.doe.gov/). For prokaryotic production, the full-length *SlFDH* coding sequence was PCR amplified from tomato cDNA using the primers SlFDH-F-pcoId and SlFDH-R-pcoId, which contained *Kpn*I and *Eco*RI restriction sites, respectively. The purified fragment was inserted into the expression vector pCold-TF. This plasmid was then introduced in *E. coli* BL21 (DE3) cells. The cells were grown to OD$_{600}$ = 0.4 at 37°C, and 0.2 mM IPTG was added to the cultures to induce protein production at 16°C for 12 h. The cells were collected and sonicated in lysis buffer. The 6*His-fusion protein was purified using Ni-NTA Beads (Smart Lifesciences) following the manufacturer's instructions (www.smart-lifesciences). Protein purity was assessed by sodium dodecyl sulfate–polyacrylamide gel electrophoresis.

The colorimetric assay was performed using 200 mM sodium phosphate (pH 7.5) containing 0.4 mg ml^{-1} nitroblue tetrazolium (NBT) and 0.03 mg ml^{-1} PMS with or without 2 μg recombinant protein, 1.62 mM NAD$^+$ and 162 mM formate (Kurt-Gür et al., 2018). In this assay, NBT receives electrons from NADH via PMS and generates blue-purple formazan. Substrate specificity was analyzed by observing the color change based on the reduction of NBT to soluble blue-purple formazan in the presence of PMS, which reacts with the NAD(P)H produced by dehydrogenases (Debnam & Shearer, 1997; Özgün et al., 2016), with the various substrates citric acid, succinic acid, DL-malic acid, sodium formate and sodium oxalate at a concentration of 50 mM. NaCl was used as a control.

The steady-state kinetic experiment was performed by detecting the absorption of NADH at 340 nm. This experiment was performed at room temperature in a reaction mixture containing 200 mM sodium phosphate at pH 7.5, 1 mM NAD$^+$, formate concentrations ranging from 0 to 168 mM, and 2 μg of purified protein or 168 mM formate, 0–2 mM NAD$^+$ and 2 μg of purified enzyme. The production of NADH was monitored by measuring the absorption at 340 nm every 20 s.

Predicted targeting of SlFDH, generation of transgenic Arabidopsis harboring *SlFDH-GFP* and subcellular localization of SlFDH

Two programs were used to predict the signal peptide of SlFDH: Plant-mPLoc: http://www.csbio.sjtu.edu.cn/cgi-bin/PlantmPLoc.cgi (Chou & Shen, 2010) and TargetP-2.0 (Emanuelsson et al., 2007).

To construct transgenic Arabidopsis lines harboring *35S: SlFDH-GFP*, a cDNA fragment of *SlFDH* containing *Xba*I and *Kpn*I restriction sites without the stop codon was amplified by PCR and cloned in the modified pCAMBIA1300 vector between the 35S promoter and *GFP*. The *35S:SlFDH-GFP* construct was introduced into Arabidopsis for stable expression by the floral dip method (Chung et al., 2000).

The fluorescence of SlFDH-GFP fusion protein and staining with a mitochondria-specific fluorescent dye (commercially available as TMRM; www.aatbio.com) were observed by confocal laser-scanning microscopy (LSM710; Carl Zeiss, Jena, Germany) as described previously (Lou, Gong, et al., 2016).

RNA extraction and qRT-PCR

Tissues were quickly excised from 1-week-old seedlings exposed to different treatments. Total RNA was extracted from the samples using an RNAprep pure Plant Kit (Tiangen). Reverse transcription was performed with 1 μg total RNA using PrimeScript RT Master Mix (Takara). qPCR was performed in a LightCycler480v machine (Roche Diagnostics, Basel, Switzerland) using SYBR Green (Toyobo). The primer sequences are listed in Table S2.

Dual-luciferase transient expression assay

To generate the *LUC* reporter constructs for the dual-luciferase assays, the coding sequences of eight TF genes (Figure 7c) lacking stop codons were separately cloned into pCAMBIA1300 under the control of the CaMV 35S promoter. The 2088-bp promoter of *SlFDH* was amplified and inserted into pGreenII 0800-LUC (Hellens et al., 2005) to generate the reporter construct. Primers are listed in Table S2. *Nicotiana benthamiana* leaves were used for dual-luciferase assays as described previously (Zhao et al., 2020). The constructs described above were transformed into *Agrobacterium* strain GV3101 (pSoup). Cultures containing empty vector or TF gene-containing effectors were co-infiltrated into *N. benthamiana* leaves along with the *proSlFDH:LUC* reporter. The infiltrated plants were cultured in a growth chamber for 3 days before examination using a NightSHADE LB985 Plant Imaging System (Berthold, Germany).

Measuring cell death

Cell death was detected by Evans blue staining as described by Yamamoto et al. (2001), with slight modifications. Briefly, intact roots were stained with 0.25% (w/v) Evans blue (BBI Life Sciences) for 30 min, washed three times with ddH$_2$O and observed under a Nikon AZ100 microscope.

Gene association analyses

Co-expression and correlation network analyses were carried out with TomExpress co-expression tools (Zouine et al., 2017). TF genes with correlation coefficients > 0.6 with *SlFDH* transcript levels were selected as candidate transcriptional regulators that might positively regulate *SlFDH*. SlSTOP1 was found to regulate *SlFDH* using PlantRegMap (Tian et al., 2020).

Electrophoretic mobility shift assay

The EMSA was performed according to Tian et al. (2021). Briefly, the coding sequence of *SlSTOP1* was cloned into pCold-TF and transformed into *E. coli* (Rosetta). After adding 0.2 mM IPTG when O.D. at 600 nm reached 0.6, the cultures were incubated at 16°C for 12 h with shaking. Proteins were purified using Ni NTA beads (SMART LIFE SCIENCE). The sequences of the predicted binding sites for SlSTOP1 were synthesized with or without biotin label, and EMSA was performed according to Tian et al. (2021) using a chemiluminescent EMSA Kit (GS009; Beyotime Biotechnology, Haimen, China).

Measurement of NAD content

One-week-old Micro-Tom seedlings were treated with or without 10 μM AlCl$_3$ for 24 h. NAD$_{total}$ (NADH + NAD$^+$) and NAD$^+$ content were detected and NADH content calculated using a WST-8 assay kit (S0175; Beyotime) according to Chamchoy et al. (2019). Briefly, after treatment, roots were collected, weighed and immediately frozen in liquid nitrogen. The roots were ground, combined with NAD$^+$/NADH lysis solution, centrifuged at 12 000 *g* for 5 min at 4°C, and the supernatant was collected. NAD$^+$ was converted to NADH using ethanol dehydrogenase. The NADH passed electrons to WST-8 via the action of PMS to produce soluble formazan, which was detected by measuring the absorbance at 450 nm. To measure NADH concentration, the samples were heated at 60°C for 30 min to degrade the NAD$^+$, and the remaining NADH was detected. To quantify the NADH contents, a NADH standard curve was constructed using a WST-8 assay kit as described above.

AUTHOR CONTRIBUTIONS

QH and JJ designed and performed the experiments, collected and analyzed the data. PL and ZW carried out protein purification. WF helped write the manuscript and discussed the results. JLY proposed and supervised the study, discussed the results, and wrote the manuscript.

CONFLICT OF INTEREST

All authors declare that they have no conflicts of interest associated with this project.

DATA AVAILABILITY STATEMENT

All relevant data can be found within the manuscript and its supporting materials.

SUPPORTING INFORMATION

Additional Supporting Information may be found in the online version of this article.

Figure S1. Multiple sequence alignment of FDH proteins.

Figure S2. Signal peptide prediction and localization of SlFDH.

Figure S3. Induction and purification of SlFDH protein.

Figure S4. Verification of different substrates by NBT color reaction.

Figure S5. Arabidopsis *FDH* promoter activity assay via transformation and GUS staining.

Figure S6. Root elongation of tomato seedlings treated with different concentrations of Al.

Figure S7. Transcriptional control of *SlFDH* predicted by the TomExpress co-expression tools.

Figure S8. Two *Slstop1* lines generated by CRISPR/Cas9 genome editing.

Figure S9. *SlFDH* expression in CRISPR/Cas9-generated *Slstop2* mutants.

Figure S10. A proposed model illustrating how SlFDH-catalyzed NAD$^+$ reduction represents an alternative pathway for NADH production.

Table S1. List of 18 genes co-expressed with *SlFDH* at the conservative threshold of correlation values greater than 0.6.

Table S2. Primers used in this study.

REFERENCES

Ambard-Bretteville, F., Small, I., Grandjean, O. & Colas Des Francs-Small, C. (2003a) Discrete mutations in the presequence of potato formate

dehydrogenase inhibit the in vivo targeting of GFP fusions into mitochondria. *Biochemical and Biophysical Research Communications*, **311**, 966–971.

Ambard-Bretteville, F., Sorin, C., Rebeille, F., Hourton-Cabassa, C. & Colas Des Francs-Small, C. (2003b) Repression of formate dehydrogenase in *Solanum tuberosum* increases steady-state levels of formate and accelerates the accumulation of proline in response to osmotic stress. *Plant Molecular Biology*, **52**, 1153–1168.

Andreadeli, A., Flemetakis, E., Axarli, I., Dimou, M., Udvardi, M.K., Katinakis, P. et al. (2009) Cloning and characterization of *Lotus japonicus* formate dehydrogenase: a possible correlation with hypoxia. *Biochimica et Biophysica Acta (BBA) - Proteins and Proteomics*, **1794**, 976–984.

Baack, R.D., Markwell, J., Herman, P.L. & Osterman, J.C. (2003) Kinetic behavior of the *Arabidopsis thaliana* leaf formate dehydrogenase is thermally sensitive. *Journal of Plant Physiology*, **160**, 445–450.

Barceló, J. & Poschenrieder, C. (2002) Fast root growth responses, root exudates, and internal detoxification as clues to the mechanisms of aluminium toxicity and resistance: a review. *Environmental and Experimental Botany*, **48**, 75–92.

Boyington, J.C., Gladyshev, V.N., Khangulov, S.V., Stadtman, T.C. & Sun, P.D. (1997) Crystal structure of formate dehydrogenase H: catalysis involving Mo, molybdopterin, selenocysteine, and an Fe_4S_4 cluster. *Science*, **275**, 1305–1308.

Bykova, N.V., Stensballe, A., Egsgaard, H., Jensen, O.N. & Moller, I.M. (2003) Phosphorylation of formate dehydrogenase in potato tuber mitochondria. *Journal of Biological Chemistry*, **278**, 26021–26030.

Chamchoy, K., Pakotiprapha, D., Pumirat, P., Leartsakulpanich, U. & Boonyuen, U. (2019) Application of WST-8 based colorimetric NAD(P)H detection for quantitative dehydrogenase assays. *BMC Biochemistry*, **20**, 4.

Che, J., Tsutsui, T., Yokosho, K., Yamaji, N. & Ma, J.F. (2018) Functional characterization of an aluminum (Al)-inducible transcription factor, ART2, revealed a different pathway for Al tolerance in rice. *New Phytologist*, **220**, 209–218.

Chen, W.W., Tang, L., Wang, J.Y., Zhu, H.H., Jin, J.F., Yang, J. et al. (2022) Research advances in the mutual mechanisms regulating response of plant roots to phosphate deficiency and aluminum toxicity. *International Journal of Molecular Science*, **23**, 1137.

Choi, D.S., Kim, N.H. & Hwang, B.K. (2014) Pepper mitochondrial *formate dehydrogenase1* regulates cell death and defense responses against bacterial pathogens. *Plant Physiology*, **166**, 1298–1311.

Chou, K.C. & Shen, H.B. (2010) Cell-PLoc 2.0: an improved package of webservers for predicting subcellular localization of proteins in various organisms. *Natural Science*, **2**, 1090–1103.

Chung, M.H., Chen, M.K. & Pan, S.M. (2000) Floral spray transformation can efficiently generate *Arabidopsis*. *Transgenic Research*, **9**, 471–486.

Dan, Y., Yan, H., Munyikwa, T., Dong, J., Zhang, Y. & Armstrong, C. (2006) MicroTom – a high-throughput model transformation system for functional genomics. *Plant Cell Reports*, **25**, 432–441.

Davison, D.C. (1951) Studies on plant formic dehydrogenase. *Biochemical Journal*, **49**, 520–526.

Debnam, P.M. & Shearer, G. (1997) Colorimetric assay for substrates of $NADP^+$-dependent dehydrogenases based on reduction of a tetrazolium dye to its soluble formazan. *Analytical Biochemistry*, **250**, 253–255.

Emanuelsson, O., Brunak, S., Heijne, G.V. & Nielsen, H. (2007) Locating proteins in the cell using TargetP, SignalP and related tools. *Nature Protocols*, **2**, 953–971.

Elisa, B., Marsano, F., Cavaletto, M. & Berta, G. (2007) Copper stress in *Cannabis sativa* roots: morphological and pro-teomic analysis. *Caryologia*, **60**, 96–101.

Fan, W., Lou, H.Q., Gong, Y.L., Liu, M.Y., Wang, Z.Q., Yang, J.L. et al. (2014) Identification of early Al-responsive genes in rice bean (*Vigna umbellata*) roots provides new clues to molecular mechanisms of Al toxicity and tolerance. *Plant, Cell & Environment*, **37**, 1586–1597.

Farinelli, M.P., Fry, D.W. & Richardson, K.E. (1983) Isolation, purification, and partial characterization of formate dehydrogenase from soybean seed. *Plant Physiology*, **73**, 858–859.

Ferry, J.G. (1990) Formate dehydrogenase. *FEMS Microbiology Letters*, **87**, 377–382.

Fukusaki, E.-I., Ikeda, T., Shiraishi, T., Nishikawa, T. & Kobayashi, A. (2000) Formate dehydrogenase gene of *Arabidopsis thaliana* is induced by

formaldehyde and not by formic acid. *Journal of Bioscience and Bioengineering*, **90**, 691–693.

Halliwell, B. (1974) Oxidation of formate by peroxisomes and mitochondria from spinach leaves. *Biochemical Journal*, **138**, 77–85.

Hanson, A.D. & Roje, S. (2001) One-carbon metabolism in higher plants. *Annual Review of Plant Physiology and Plant Molecular Biology*, **52**, 119–137.

Hellens, R.P., Allan, A.C., Friel, E.N., Bolitho, K., Grafton, K., Templeton, M.D. et al. (2005) Transient expression vectors for functional genomics, quantification of promoter activity and RNA silencing in plants. *Plant Methods*, **1**, 13.

Herman, P.L., Ramberg, H., Baack, R.D., Markwell, J. & Osterman, J.C. (2002) Formate dehydrogenase in *Arabidopsis thaliana*: overexpression and subcellular localization in leaves. *Plant Science*, **163**, 1137–1145.

Hoagland, D.R. & Arnon, D.I. (1950) The water-culture method for growing plants without soil. *California Agricultural Experiment Station Circular*, **347**, 1– 39.

Hourton-Cabassa, C., Ambard-Bretteville, F., Moreau, F., de Virville, J.D., Remy, R. & Colas Des Francs-Small, C. (1998) Stress induction of mitochondrial formate dehydrogenase in potato leaves. *Plant Physiology*, **116**, 627–635.

Hradilová, J., Řehulka, P., Řehulková, H., Vrbová, M., Griga, M. & Brzobohatý, B. (2010) Comparative analysis of proteomic changes in contrasting flax cultivars upon cadmium exposure. *Electrophoresis*, **31**, 421–431.

Iida, M., Kitamura-Kimura, K., Maeda, H. & Mineki, S. (1992) Purification and characterization of a NAD^+-dependent formate dehydrogenase produced by *Paracoccus* sp. *Bioscience, Biotechnology, and Biochemistry*, **56**, 1966–1970.

Iuchi, S., Koyama, H., Iuchi, A., Kobayashi, Y., Kitabayashi, S., Kobayashi, Y. et al. (2007) Zinc finger protein STOP1 is critical for proton tolerance in *Arabidopsis* and coregulates a key gene in aluminum tolerance. *Proceedings of the National Academy of Sciences of the United States of America*, **104**, 9900–9905.

Jin, J.F., Wang, Z.Q., He, Q.Y., Wang, J.Y., Li, P.F., Xu, J.M. et al. (2020) Genome-wide identification and expression analysis of the NAC transcription factor family in tomato (*Solanum lycopersicum*) during aluminum stress. *BMC Genomics*, **21**, 288.

Jin, J.F., Zhu, H.H., He, Q.Y., Li, P.F., Fan, W., Xu, J.M. et al. (2022) The tomato transcription factor SINAC063 is required for aluminum tolerance by regulating *SlAAE3-1* expression. *Frontiers in Plant Science*, **13**, 826954.

Kobayashi, Y., Ohyama, Y., Kobayashi, Y., Ito, H., Iuchi, S., Fujita, M. et al. (2014) STOP2 activates transcription of several genes for Al- and low pH-tolerance that are regulated by STOP1 in Arabidopsis. *Molecular Plant*, **7**, 311–322.

Kochian, L.V., Piñeros, M.A., Liu, J.P. & Magalhaes, J.V. (2015) Plant adaptation to acid soils: the molecular basis for crop aluminum resistance. *Annual Review of Plant Biology*, **66**, 571–598.

Kurt-Gür, G., Demirci, H., Sunulu, A. & Ordu, E. (2018) Stress response of NAD^+-dependent formate dehydrogenase in *Gossypium hirsutum* L. grown under copper toxicity. *Environmental Science & Pollution Research*, **25**, 31679–31690.

Labrou, N.E. & Rigden, D.J. (2001) Active-site characterization of *Candida boidinii* formate dehydrogenase. *Biochemical Journal*, **354**, 455–463.

Li, R., Moore, M., Bonham-Smith, P.C. & King, J. (2002) Overexpression of formate dehydrogenase in *Arabidopsis thaliana* resulted in plants tolerant to high concentrations of formate. *Journal of Plant Physiology*, **159**, 1069–1076.

Li, R., Ziola, B. & King, J. (2000) Purification and characterization of formate dehydrogenase from *Arabidopsis thaliana*. *Journal of Plant Physiology*, **157**, 161–167.

Lou, H.Q., Fan, W., Xu, J.M., Gong, Y.L., Jin, J.F., Chen, W.W. et al. (2016) An oxalyl-CoA synthetase is involved in oxalate degradation and aluminum tolerance. *Plant Physiology*, **172**, 1679–1690.

Lou, H.Q., Gong, Y.L., Fan, W., Xu, J.M., Liu, Y., Cao, M.J. et al. (2016) A formate dehydrogenase confers tolerance to aluminum and low pH. *Plant Physiology*, **171**, 294–305.

Mathews, M.B. & Vennesland, B. (1950) Enzymic oxidation of formic acid. *Journal of Biological Chemistry*, **186**, 667–682.

McNeilly, D., Schofield, A. & Stone, S.L. (2018) Degradation of the stress-responsive enzyme formate dehydrogenase by the RING-type E3 ligase keep on going and the ubiquitin 26 S proteasome system. *Plant Molecular Biology*, **96**, 265–278.

Nanba, H., Takaoka, Y. & Hasegawa, J. (2003) Purification and characterization of formate dehydrogenase from *Ancylobacter aquaticus* strain KNK607M, and cloning of the gene. *Bioscience, Biotechnology, and Biochemistry*, **67**, 720–728.

Olson, B.J.S.C., Skavdahl, M., Ramberg, H., Osterman, J.C. & Markwell, J. (2000) Formate dehydrogenase in *Arabidopsis thaliana*: characterization and possible targeting to the chloroplast. *Plant Science*, **159**, 205–212.

Özgün, G.P., Ordu, E.B., Tütüncü, H.E., Yelboğa, E., Sessions, R.B. & Karagüler, N.G. (2016) Site saturation mutagenesis applications on *Candida methylica* formate dehydrogenase. *Scientifica*, **2016**, 4902450.

Peacock, D. & Boulter, D. (1970) Kinetic studies of formate dehydrogenase. *Biochemical Journal*, **120**, 763–769.

Prabhu, V., Chatson, K.B., Abrams, G.D. & King, J. (1996) ^{13}C nuclear magnetic resonance detection of interactions of serine hydroxymethyltransferase with C1-tetrahydrofolate synthase and glycine decarboxylase complex activities in *Arabidopsis*. *Plant Physiology*, **112**, 207–216.

Sawaki, Y., Iuchi, S., Kobayashi, Y., Kobayashi, Y., Ikka, T., Sakurai, N. et al. (2009) STOP1 regulates multiple genes that protect *Arabidopsis* from proton and aluminum toxicities. *Plant Physiology*, **150**, 281–294.

Shiraishi, T., Fukusaki, E.-I. & Kobayashi, A. (2000) Formate dehydrogenase in rice plant: growth stimulation effect of formate in rice plant. *Journal of Bioscience and Bioengineering*, **89**, 241–246.

Small, I., Peeters, N., Legeai, F. & Lurin, C. (2004) Predotar: a tool for rapidly screening proteomes for N-terminal targeting sequences. *Proteomics*, **4**, 1581–1590.

Suzuki, K., Itai, R., Suzuki, K., Nakanishi, H., Nishizawa, N.K., Yoshimura, E. et al. (1998) Formate dehydrogenase, an enzyme of anaerobic metabolism, is induced by iron deficiency in barley roots. *Plant Physiology*, **116**, 725–732.

Tian, F., Yang, D.C., Meng, Y.Q., Jin, J.P. & Gao, G. (2020) PlantRegMap: charting functional regulatory maps in plants. *Nucleic Acids Research*, **48**, 1104–1113.

Tian, W.H., Ye, J.Y., Cui, M.Q., Chang, J.B., Liu, Y., Li, G.X. et al. (2021) A transcription factor STOP1-centered pathway coordinates ammonium and phosphate acquisition in Arabidopsis. *Molecular Plants*, **14**, 1554–1568.

Tishkov, V.I. & Popov, V.O. (2004) Catalytic mechanism and application of formate dehydrogenase. *Biochemistry*, **69**, 1252–1267.

Vinals, C., Depiereux, E. & Feytmans, E. (1993) Prediction of structurally conserved regions of D-specific hydroxy acid dehydrogenases by multiple alignment with formate dehydrogenase. *Biochemical and Biophysical Research Communications*, **192**, 182–188.

Wang, R., Zeng, Z.D., Guo, H.X., Tan, H., Liu, A., Zhao, Y. et al. (2018) Over-expression of the *Arabidopsis* formate dehydrogenase in chloroplasts enhances formaldehyde uptake and metabolism in transgenic tobacco leaves. *Planta*, **247**, 339–354.

Xian, P.Q., Cai, Z.D., Cheng, Y.B., Lin, R.B., Lian, T.X., Ma, Q.B. et al. (2020) Wild soybean oxalyl-CoA synthetase degrades oxalate and affects the tolerance to cadmium and aluminum stresses. *International Journal of Molecular Science*, **21**, 8869.

Xu, J.M., Fan, W., Jin, J.F., Lou, H.Q., Chen, W.W., Yang, J.L. et al. (2017) Transcriptome analysis of Al-induced genes in buckwheat (*Fagopyrum esculentum* moench) root apex: new insight into al toxicity and resistance mechanisms in an al accumulating species. *Frontiers in Plant Science*, **8**, 1141.

Yamamoto, Y., Kobayashi, Y. & Matsumoto, H. (2001) Lipid peroxidation is an early symptom triggered by aluminum, but not the primary cause of elongation inhibition in pea roots. *Plant Physiology*, **125**, 199–208.

Yang, J.L., Fan, W. & Zheng, S.J. (2019) Mechanisms and regulation of aluminum-induced secretion of organic acid anions from plant roots. *Journal of Zhejiang University-Science B*, **20**, 513–527.

Zhang, L., Dong, D., Wang, J., Zhang, J., Bai, R.-Y., Wang, X. et al. (2022) A zinc finger protein SlSZP1 protects SlSTOP1 from SlRAE1-mediated degradation to modulate aluminum resistance. *New Phytologist*, **236**, 165–181.

Zhang, Y., Zhang, J., Guo, J., Zhou, F., Singh, S., Xu, X. et al. (2019) F-box protein RAE1 regulates the stability of the aluminum-resistance transcription factor STOP1 in *Arabidopsis*. *Proceedings of the National Academy of Sciences of the United States of America*, **116**, 319–327.

Zhao, J.M., Zhang, Y.M., Bian, X., Lei, J., Sun, J.T., Guo, N. et al. (2013) A comparative proteomics analysis of soybean leaves under biotic and abiotic treatments. *Molecular Biology Reports*, **40**, 1553–1562.

Zhao, X.Y., Qi, C.H., Jiang, H., Zhong, M.S., You, C.X., Li, Y.Y. et al. (2020) MdWRKY15 improves resistance of apple to *Botryosphaeria dothidea* via the salicylic acid-mediated pathway by directly binding the *MdICS1* promoter. *Journal of Integrative Plant Biology*, **62**, 527–543.

Zheng, S.J. & Yang, J.L. (2005) Target sites of aluminum phytotoxicity. *Biologia Plantarum*, **49**, 321–331.

Zouine, M., Maza, E., Djari, A., Lauvernier, M., Frasse, P., Smouni, A. et al. (2017) TomExpress, a unified tomato RNA-Seq platform for visualization of expression data, clustering and correlation networks. *The Plant Journal*, **92**, 727–735.